# Charge Resonance and Photoinduced Charge Transfer in Bis(N, N-Dimethylaminophenyl-TCBD)-Diketopyrrolopyrrole Multi-Modular System

Charu Popli, a,‡ Youngwoo Jang, b,‡ Rajneesh Misra\* and Francis D'Souzab\*

<sup>a</sup>Department of Chemistry, Indian Institute of Technology, Indore 453552, India. E-mail: <a href="mailto:rajneeshmisra@iiti.ac.in">rajneeshmisra@iiti.ac.in</a>

<sup>b</sup>Department of Chemistry, University of North Texas, 1155 Union Circle, #305070, Denton, TX 76203-5017, USA, E-mail: Francis.DSouza@UNT.edu

Abstract: Intervalence charge transfer (IVCT) or charge resonance, is often observed in redoxactive systems encompassed of two identical electroactive groups and when one of the groups is either oxidized or reduced and serves as a model system to improve our fundamental understanding of charge transfer. This property has been explored in the present study in a multi-modular pushpull system carrying two N, N-dimethylaminophenyl-tetracyanobutadiene (DMA-TCBD) entities covalently linked to the opposite ends of bis(thiophenyl)diketopyrrolopyrrole (TDPP). Electrochemical or chemical reduction of one of the TCBDs promoted electron resonance between them exhibiting an IVCT absorption peak in the near-infrared (NIR) area. The comproportionation energy,  $-\Delta G_{\text{com}}$  and equilibrium constant,  $K_{\text{com}}$  evaluated from the split reduction peak were, respectively, 1.06 x 10<sup>4</sup> J/mol, and 72.3 M<sup>-1</sup>. Excitation of the TDPP entity in the system promoted the thermodynamically feasible sequential charge transfer and separation of charges in benzonitrile wherein the IVCT peak formed upon charge separation served as a signature peak in characterizing the product. Further, transient data analyzed using Global Target Analysis (GloTarAn) revealed the charge separation to take place in ps  $(k \sim 10^{10} \, \text{s}^{-1})$  time scale as a result of close positioning and strong electronic interaction between the entities. The significance of IVCT in probing excitedstate processes is evidenced by the present study.

<sup>‡</sup>Equal contribution

# Introduction

Intervalence charge transfer (IVCT), also known as charge resonance, is seen in molecular systems carrying two identical electro-active sites connected by a spacer (Sp) and differing in their redox state by one.<sup>1-20</sup> Such IVCT-exhibiting model compounds are key to exploring the fundamentals of electron transfer targeted for a range of applications, especially in the area of single-molecule electronics.<sup>21-23</sup> The first known compounds exhibiting this property are the classical bis-Ruthenium Creutz-Taube type inorganic complexes, however, a range of inorganic as well as organic systems have been constructed and studied to explore this phenomenon. 1-3 The nature of IVCT depends on charge localization and delocalization in the mixed valance state, viz., complete localization, full delocalization, and anything in between. The completely localized systems are abbreviated as  $R^{n+}$ -Sp- $R^{(n+1)+}$  where the charge is confined to a given redox center, while the fully delocalized systems are abbreviated as  $R^{(n+0.5)+}$ -Sp- $R^{(n+0.5)+}$  where the odd electron is equally distributed among the redox centers. In the third class, partial electron delocalization occurs. According to Robin and Day's arrangement,<sup>24</sup> the completely confined systems are termed as class I, fully delocalized systems as class III, and class II belonging to systems whose behavior is in between type I and type III. Class II systems exhibit a solvent polarity-dependent IVCT Gaussianshaped peak in the NIR region of the electromagnetic spectrum while IVCT peak in class III type systems is asymmetrical and largely solvent independent. 25, 26

Highly interacting electron push-pull systems comprised of closely connected electron-rich and electron-deficient molecules as part of the same molecule or two separated ones, often exhibit absorption band(s) in the visible/near-IR regions due to charge polarization, also called ground state intramolecular charge transfer (ICT). These bands differ from the traditional  $\pi$ - $\pi$ \* transitions of the parent  $\pi$ -systems (called locally excited, LE). Synthesis of one of the elegant push-pull systems involves incorporating strong electron acceptors, tetracyanoethylene (TCNE) or tetracyano-quinodimethane (TCNQ), via a cycloaddition-retroelectrocyclization reaction involving ethynyl-donors. This reaction is facile and occurs without the help of any catalyst. The resulting donor-tetracyanobutadiene (TCBD) and donor-dicyanodiquinodimethane (DCNQ) are known to exhibit strong charge polarization in the ground state and ultrafast excited state charge transfer as a consequence of strong push-pull effect exerted in them. Noteworthy studies have

appeared in the literature on such push-pull systems developed following this approach, and a majority of them have been shown to undergo charge transfer upon photoexcitation. 43-53

For building donor-TCBD and donor-DCNQ multi-modular systems, often a photosensitizer-donor entity having absorption and emission in the visible region is coupled to promote the excited-state charge transfer by visible light irradiation. Photosensitizers such as porphyrins, phthalocyanines, BODIPYs, azaBODIPYs, subphthalocyanine, phenothiazine, and triphenylamine, etc. are some of the targeted sensitizers. In addition to these sensitizers, recently, the TDPP derivatives have also been employed.<sup>54-64</sup> The TDPPs are appealing as they can be subjected to further modification to introduce additional functionalities to enhance their photo-and electrochemical properties.<sup>65-71</sup> Not surprisingly, nowadays, these are commonly used in materials exhibiting singlet fission,<sup>66</sup> photovoltaics,<sup>54</sup> and field-effect transistor properties.<sup>58</sup>

#### Previously studied system

#### **Currently studied systems**

*Figure 1*. Structure and abbreviations of the previously reported and currently developed pushpull systems to witness IVCT and excited-state charge transfer.

Recently, we reported a bis-functionalized TDPP carrying two entities of phenothiazine-TCBD entities, labeled as (PTZ-TCBD)<sub>2</sub>-TDPP in Figure 1.<sup>72</sup> Electroreduction of one of the TCBD entities in (PTZ-TCBD)<sub>2</sub>-TDPP triggered electron resonance between the TCBD entities exhibiting IVCT in the NIR region. Further, such a signature peak was useful to characterize the product of the excited-state charge transfer. Encouraged by these findings, in the present study, we have extended the molecular design keeping the central TDPP and TCBD the same, but replacing the PTZ entities with another electron donor, N,N-dimethylaniline (DMA), (abbreviated as (DMA-TCBD)<sub>2</sub>-TDPP, 1 in Figure 1). By this, we would like to address a key question of whether the terminal electron donors modulate the IVCT and the subsequent CT events, and if so, to what extent. To address such a relatively complex question, a series of control compounds displayed in Figure 1 and systematic studies on them were also warranted. In this series, 2 and 3 made of a single DMA-TCBD are controls required to prove IVCT transition in 1 upon reducing one of the DMA-TCBD entities. The lack of a second TCBD in 2 and 3 is expected not to show IVCT transition upon electroreduction. Importantly, owing to the presence of electron rich DMA and electron poor TCBD in 2 and 3 these could show an ICT band in the visible region. Compound 4 has only DMA and TCBD entities without TDPP. This compound is to show that the ICT is primarily due to the push-pull effect caused by DMA-TCBD. The next set of control compounds, 5 and 6 have no TCBD, hence, the absence of ICT in the ground state or IVCT upon electroreduction could be expected. Finally, compound 7 is a reference TDPP lacking DMA (phenyl rings instead of N,N-dimethylaniline) needed to spectrally and electrochemically characterize peripherally functionalized TDPP. Our findings show that the IVCT characteristics are primarily governed by the TCBD-TDPP-TCBD framework in 1 with some contributions from the terminal electron donor entities.

# **Experimental Section**

# **Synthesis: General Strategy**

Scheme 1 depicts the synthetic methodology used for 1, (DMA-TCBD)<sub>2</sub>-TDPP, and the control compounds while details are given below. Using palladium-catalyzed Sonogashira cross-coupling reaction of **DPP 1** with 1.0 equivalent of 4-ethynyl-*N*, *N*-dimethylaniline, and **DPP 2** 

with 2.0 equivalent of 4-ethynyl-*N*, *N*-dimethylaniline, **5** and **6** were synthesized in 60% and 70% yields (Scheme 1). The [2+2] cycloaddition-electrocyclic ring-opening reaction of compound **5** with 1.0 equivalent of TCNE resulted in **3** in 85 % yield. Similarly, compound **6** on reaction with 1.0 and 2.0 equivalent of TCNE yielded **2** and **1** in 75% and 90% yields, respectively. Further, the synthesized compounds were purified by column chromatography over silica gel and additional recrystallization techniques. The existence of the two N-C<sub>10</sub> alkyl chains on TDPP helped increase the solubility of these compounds in most of the common organic solvents. The structural assessment of the final compounds was arrived at by a combination of <sup>1</sup>H and <sup>13</sup>C NMR and HRMS techniques (see Figures S1-S21 in the SI for spectral characterization data).

**Scheme 1.** The methodology used in the preparation of 1, (DMA-TCBD)<sub>2</sub>-TDPP along with the control compounds.

#### **Synthesis of 5**

**DPP 1** (0.250 g, 0.37 mmol) and 4-ethynyl-*N*, *N*-dimethylaniline (0.080 g, 0.55 mmol) were dissolved in a round bottom flask containing anhydrous toluene (25 mL) and triethylamine (1 mL). The mixture was then degassed under an inert atmosphere for 20 min followed by the addition of Pd(PPh<sub>3</sub>)<sub>4</sub> (0.017 g, 0.015 mmol), and CuI (0.006 g, 0.030 mmol). The reaction mixture was stirred for 12 h at 80 °C. The reaction mixture was then cooled down to room temperature after the

completion of the reaction. The solvent was removed under vacuum and the crude product was purified by repeated silica gel column chromatography with hexane/DCM (3:2) as an eluent to get 5 in 60% yield.

<sup>1</sup>H NMR (400 MHz, CDCl<sub>3</sub>, δ in ppm): 8.93 (2H, m), 8.66 (1H, m), 7.62 (1H, d), 7.39 (2H, m), 7.31 (1H, m), 6.66 (1H, m), 6.56 (1H, m), 4.02 (4H, m), 2.88 (6H, m), 1.73 (4H, m), 1.33 (28H, m), 0.86 (6H, m); <sup>13</sup>C NMR (100 MHz, CDCl<sub>3</sub>, δ in ppm): 161.4, 161.2, 150.6, 139.6, 139.5, 135.8, 135.2, 133.1,132.9, 131.9, 130.6, 130.2, 129.9, 129.3, 128.6, 112.0, 111.7, 108.6, 108.0, 107.9, 80.8, 42.3, 40.1, 31.9, 30.1, 30.0, 29.5, 29.3, 29.2, 26.9, 22.7, 14.1; HRMS m/z calcd for C<sub>44</sub>H<sub>57</sub>N<sub>3</sub>O<sub>2</sub>S<sub>2</sub>: 746.3784 [M+Na<sup>+</sup>], found 746.3282; UV/vis (Dichloromethane)  $\lambda_{max}$  585 nm,  $\epsilon$  [M<sup>-1</sup>cm<sup>-1</sup>] (1.48×10<sup>4</sup>).

# Synthesis of 3

**5** (0.100 g, 0.138 mmol) and tetracyanoethylene (0.026 g, 0.207 mmol) were dissolved in a 100 mL round bottom flask containing anhydrous DCM under an inert atmosphere. The reaction mixture was allowed to be stirred for 15 minutes at room temperature. The solvent was removed under vacuum and the crude product was purified by repeated silica gel column chromatography with hexane/DCM (1:4) as an eluent to get **3** in 85% yield.

<sup>1</sup>H NMR (400 MHz, CDCl<sub>3</sub>, δ in ppm): 8.96 (2H, s), 7.41 (4H, d), 7.31 (2H, s), 6.65 (4H, m), 4.09 (4H, s), 3.02 (12H,s), 1.76 (4H, s), 1.35 (28H, m), 0.87 (6H, s); <sup>13</sup>C NMR (100 MHz, CDCl<sub>3</sub>, δ in ppm): 161.2, 150.6, 139.0, 135.7, 132.9, 131.9, 130.1, 129.4, 111.7, 108.7, 108.3, 100.0, 80.9, 42.4, 40.1, 31.9, 30.1, 29.6, 29.3, 26.9, 22.7, 14.1; HRMS m/z calcd for C<sub>54</sub>H<sub>66</sub>N<sub>4</sub>O<sub>2</sub>S<sub>2</sub>: 889.4519 [M+Na<sup>+</sup>], found 889.4521; UV/vis (Dichloromethane)  $\lambda_{max}$  632 nm,  $\epsilon$  [M<sup>-1</sup>cm<sup>-1</sup>] (4.72×10<sup>4</sup>).

# Synthesis of 6

**DPP 2** (0.250 g, 0.34 mmol) and 4-ethynyl-*N*, *N*-dimethylaniline (0.122 g, 0.84 mmol) were dissolved in a round bottom flask containing anhydrous toluene (25 mL) and triethylamine (10 mL). The reaction mixture was degassed with inert gas for 20 min followed by the addition of Pd(PPh<sub>3</sub>)<sub>4</sub> (0.017 g, 0.015 mmol), and CuI (0.006 g, 0.030 mmol). The reaction mixture was stirred 12 h at 80°C. The reaction mixture was allowed to cool down at room temperature after the completion of the reaction. The solvent was removed under vacuum and the crude product was

purified by repeated silica gel column chromatography with hexane/DCM (3:2) as an eluent to get 6 in 70% yield.

<sup>1</sup>H NMR (400 MHz, CDCl<sub>3</sub>, δ in ppm): 9.16 (1H, d), 9.02 (1H, d), 7.78 (4H, m), 7.34 (1H, s), 6.71 (2H, d), 4.07 (4H, s), 3.17 (6H, s), 1.72 (4H, m), 1.41 (28H, m), 0.87 (6H, m); <sup>13</sup>C NMR (100 MHz, CDCl<sub>3</sub>, δ in ppm): 162.0, 161.4, 160.6, 157.9, 154.6, 143.9, 139.9, 137.9, 137.3, 135.6, 135.1, 133.3, 132.5, 129.2, 117.7, 114.2, 113.3, 113.1, 112.7, 112.3, 111.9, 108.4, 80.1, 42.7, 42.5, 40.2, 31.9, 30.4, 29.8, 29.5, 29.3, 29.2, 26.8, 22.7, 14.2, 14.1; HRMS m/z calcd for C<sub>50</sub>H<sub>57</sub>N<sub>7</sub>O<sub>2</sub>S<sub>2</sub>: 874.3907 [M+Na<sup>+</sup>], found 874.3336; UV/vis (Dichloromethane)  $\lambda_{max}$  678 nm,  $\epsilon$  [M<sup>-1</sup>cm<sup>-1</sup>] (1.11×10<sup>4</sup>).

#### Synthesis of 2

**6** (0.100 g, 0.11 mmol) and tetracyanoethylene (0.018 g, 0.14 mmol) were dissolved in a 50 mL round bottom flask containing anhydrous DCM under an inert atmosphere. The reaction mixture was allowed to be stirred for 10 minutes at room temperature. The solvent was removed under vacuum and the crude product was purified by repeated silica gel column chromatography with hexane/DCM (1:4) as an eluent to get **2** in 75% yield.

<sup>1</sup>H NMR (400 MHz, CDCl<sub>3</sub>, δ in ppm): 9.20 (1H, d), 9.03 (1H, d), 7.78 (3H, m), 7.42 (2H, m), 7.35 (1H, m), 6.68 (4H, m), 4.07 (4H, d), 3.17 (3H, s), 3.07 (3H, s), 1.75 (4H, s), 1.33 (28H, m), 0.86 (6H, m); <sup>13</sup>C NMR (100 MHz, CDCl<sub>3</sub>, δ in ppm): 162.0, 161.4, 160.3, 157.6, 154.5, 150.8, 143.1, 140.1, 138.7, 138.6, 137.9, 137.0, 135.07, 135.02, 134.8, 133.5, 133.4, 133.2, 133.0, 132.7, 132.6, 128.4, 117.8, 114.2, 113.3, 113.2, 113.1, 112.4, 112.0, 111.9, 111.8, 111.7, 108.7, 108.0, 102.6, 42.8, 42.7, 40.4, 40.0, 32.1, 32.0, 31.9, 30.5, 30.4, 30.3, 29.9, 29.8, 29.7, 27.0, 26.9, 26.8, 22.9, 22.8, 22.7, 14.3, 14.1; HRMS m/z calcd for  $C_{60}H_{66}N_8O_2S_2$ : 994.4745 [M<sup>+</sup>], found 994.4227; UV/vis (Dichloromethane)  $λ_{max}$  731 nm, ε [M<sup>-1</sup>cm<sup>-1</sup>] (0.61×10<sup>4</sup>).

### Synthesis of 1

6 (0.100 g, 0.11 mmol) and tetracyanoethylene (0.035 g, 0.27 mmol) were dissolved in a 50 mL round bottom flask containing anhydrous DCM under an inert atmosphere. The reaction mixture was allowed to stir for 15 minutes at room temperature. The solvent was removed under vacuum

and the crude product was purified by repeated silica gel column chromatography with hexane/DCM (1:9) as an eluent to get 1 in 90% yield.

<sup>1</sup>H NMR (400 MHz, CDCl<sub>3</sub>, δ in ppm): 9.14 (2H, d), 7.78 (6H, m), 6.72 (4H, m), 4.06 (4H, m), 3.18 (12H, s), 1.71 (4H, m), 1.25 (28H, m), 0.87 (6H, m); <sup>13</sup>C NMR (100 MHz, CDCl<sub>3</sub>, δ in ppm): 161.5, 160.6, 158.0, 154.6, 139.4, 139.1, 138.5, 136.8, 132.5, 117.6, 114.1, 113.3, 112.8, 112.7, 112.4, 111.5, 81.8, 42.9, 40.3, 31.9, 30.3, 29.5, 29.3, 29.2, 26.8, 22.7, 14.1; HRMS m/z calcd for  $C_{66}H_{66}N_{12}O_2S_2$ : 1145.4765 [M+Na<sup>+</sup>], found 1145.4892; UV/vis (Dichloromethane)  $\lambda_{max}$  735 nm,  $\epsilon$  [M<sup>-1</sup>cm<sup>-1</sup>] (1.72×10<sup>4</sup>).

## Synthesis of 4

In a 100 mL round bottom flask, 4-ethynyl-*N*, *N*-dimethyl aniline (0.150 g, 1.03 mmol), and 2-bromo thiophene (0.202, 1.2 mmol) in 25 mL toluene and 10 mL triethylamine was dissolved. The reaction mixture was degassed with argon for 20 min followed by the addition of Pd(PPh<sub>3</sub>)<sub>4</sub> (0.017 g, 0.015 mmol), and CuI (0.006 g, 0.030 mmol). The reaction mixture was stirred for 12 h at 80°C. The reaction mixture was allowed to cool down at room temperature after the completion of the reaction. The solvent was removed under vacuum and the crude product was purified by repeated silica gel column chromatography with hexane/DCM (3:2) as an eluent to get **8** in 72% yield. **8** (0.08 g, 0.35 mmol) and TCNE (0.054 g, 0.42 mmol) were dissolved in anhydrous DCM in an inert atmosphere. The reaction mixture was allowed to stir for 1h at room temperature. The solvent was removed under vacuum and the crude product was purified by repeated silica gel column chromatography with hexane/DCM (2:3) as an eluent to get **4** in 92% yield.

<sup>1</sup>H NMR (400 MHz, CDCl<sub>3</sub>, δ in ppm): 7.91 (2H, m), 7.77 (2H, m), 7.28 (1H, m), 6.72 (2H, m), 3.16 (6H, s); <sup>13</sup>C NMR (100 MHz, CDCl<sub>3</sub>, δ in ppm): 162.4, 159.8, 154.5, 137.9, 137.1, 135.5, 132.5, 129.8, 117.7, 114.3, 113.2, 112.8, 112.2, 111.7, 80.3, 74.6, 53.4, 40.2, 29.7. HRMS m/z calcd for  $C_{20}H_{13}N_3S$ : 356.0998 [M+H<sup>+</sup>], found 356.0964.

#### Synthesis of 7

In a 100 ml round bottom flask, **DPP 2** (0.100 g, 0.146 mmol) and ethynylbenzene (0.039 mg, 0.380 mmol) were dissolved in 15 mL dry THF and 5 mL of triethylamine was added to this solution. The reaction mixture was degassed with nitrogen for 10 minutes and then Pd(PPh<sub>3</sub>)<sub>2</sub>Cl<sub>2</sub>

(20 mg, 0.0292 mmol), triphenylphosphine (2 mg) and copper(I) iodide (3 mg) were added. The reaction mixture was refluxed for 12 hours at 80 °C. After completion of the reaction, the reaction mixture was allowed to cool down to room temperature. The solvents were removed under vacuum and the crude was purified by column chromatography using hexane: dichloromethane (3:2) as an eluent to give compound 7 in 68 % yield.

<sup>1</sup>H NMR (400 MHz, CDCl<sub>3</sub>,  $\delta$  in ppm): 8.95 (2H, m), 7.55 (4H, m), 7.38 (8H, m), 4.07 (4H, m), 1.76 (4H, m), 1.38 (8H, m), 1.35 (20H, m), 1.27 (6H, m); <sup>13</sup>C NMR (100 MHz, CDCl<sub>3</sub>,  $\delta$  in ppm): 161.2, 139.1, 135.6, 133.1, 131.6, 130.4, 129.1, 128.7, 128.5, 122.2, 108.7, 97.8, 82.3, 42.4, 31.9, 30.08, 29.5, 29.3, 26.9, 22.7, 14.1; HRMS m/z calcd for C<sub>50</sub>H<sub>56</sub>N<sub>2</sub>O<sub>2</sub>S<sub>2</sub>: 803.3675 [M+Na<sup>+</sup>], found 803.3279.

# **Results and Discussion**

## Absorption and fluorescence studies

The normalized optical absorption spectrum of the investigated compounds in benzonitrile is shown in Figure 2a. The phenyl ethynyl functionalized TDPP, 7, lacking either DMA or TCBD, revealed peaks at 573 and 619 nm. The TDPP lacking molecular entity 4 featuring DMA and TCBD entities, revealed two peaks at 480 and 535 nm. From comparison with previous studies of this class of compounds, <sup>43-51</sup> the 535 nm peak has been attributed to ICT transition. For compounds 5 and 6 having one and two DMAs linked to the central TDPP, the spectral attributes were close to that of 7, however, with notable differences. For 5 having only one DMA group, the peak maxima were blue-shifted by 13 and 27 nm when compared to the corresponding peaks of 7 due to the lack of one of the ethynyl entities. In Compound 6 with two DMA entities attached to TDPP, these peaks were bathochromically shifted by about 10 nm suggesting some intramolecular interactions. Finally, for 1-2, where one and two ICT exhibiting DMA-TCBD entities were in existence, bathochromically moved spectra were observed. Peak maxima at 745 nm for 1 and 742 nm for 2 were noted. In the case of 3, having only one DMA-TCBD, the absorption band was located at 687 nm, however, compared to 5 (its control compound lacking TCBD acceptor), this band was bathochromically moved by 47 nm due to ICT originating in DMA-TCBD. The spectral data are given in Table 1 which demonstrates the effect of varying numbers of  $\pi$ -extending ethynyl arms, donor DMAs, and ICT DMA-TCBDs on the central TDPP in modulating spectral features.

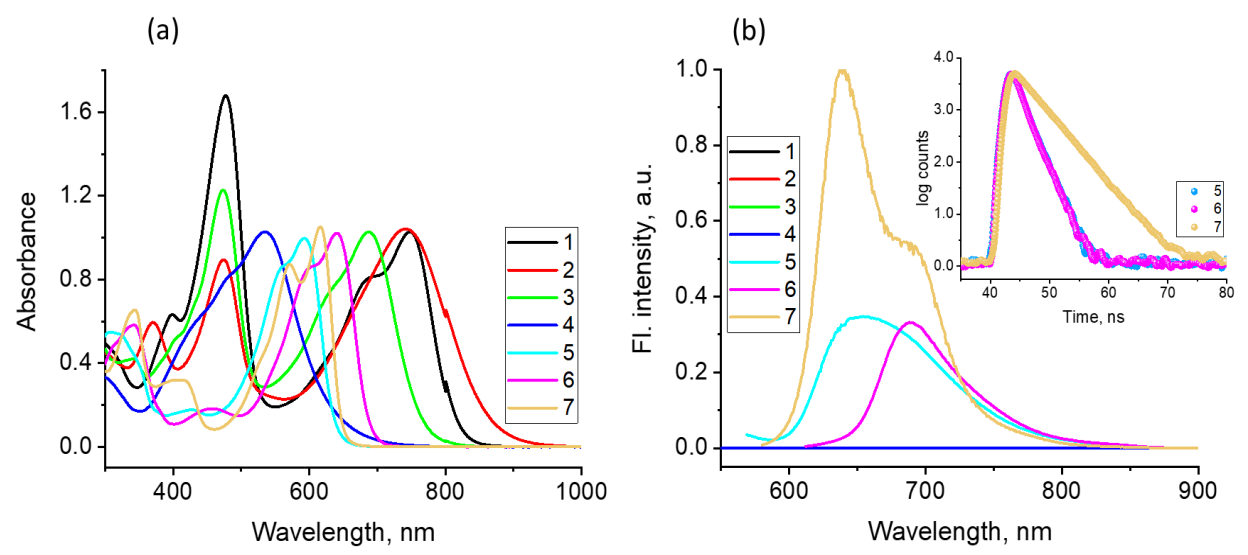


*Figure 2*. (a) Visible/near-IR absorption and (b) fluorescence emission spectra of the studied systems in PhCN. In Figure 2b, the samples were excited at the low energy visible peak maxima shown in Table 1. The singlet decay profiles from TCSPC of 5, 6, and 7 are shown in the inset of Figure 2b.

Figure 2b shows the singlet emission spectrum of the studied compounds, excited at their low-energy visible peak maxima (see Table 1). Lack of emission from TDPP systems connected to electron-poor TCBDs (1 to 3) was observed signifying the occurrence of nonradiative processes.<sup>73</sup> Similarly, no fluorescence from compound 4 lacking TDPP was also observed. On the contrary, compounds 5-7 revealed fluorescence emission from the TDPP entity. The control compound 7, lacking any electron-rich DMA entities revealed fluorescence at 642 and 669 nm. For compound 6 having DMA entities instead of phenyl rings, the main peak was found to be quenched and bathochromically shifted to 688 nm. Similarly, the peak was quenched for compound 5 having only one DMA entity, and appeared at 654 nm. Such a trend was also observed in the measured fluorescence lifetimes. Fluorescence decays from time-correlated single-photon counting (TCSPC) method by using pulsed nanoLED excitation were monoexponential for both 6 and 7 (decay profiles are shown in Figure 2b inset). The lifetime of 7 having no DMA was 3.01 ns while that of 6 with two DMAs it was 1.31 ns, and for 5 with one DMA, it was 1.35 ns. The reduced singlet emission lifetimes and intensities in 5 and 6 suggest photoinduced events, likely excited state charge transfer involving the slightly electron-deficient TDPP and electron-rich DMA moieties (vide supra).

Table 1. Absorption and fluorescence emission peak maxima, electrochemical oxidation and reduction potentials, and Gibbs energy changes for charge transfer and separation, and solvation in PhCN.

|          |                       | Potential V vs. Ag/AgCl |     |     |                       |                     |                  |      |       |                 |       |         |                         |                         |                          |                           |      |      |
|----------|-----------------------|-------------------------|-----|-----|-----------------------|---------------------|------------------|------|-------|-----------------|-------|---------|-------------------------|-------------------------|--------------------------|---------------------------|------|------|
| Compound | $\lambda_{abs'}$ , nm |                         |     |     | $\lambda_{_{Em'}}$ nm | τ <sub>Fl</sub> , - | E <sub>red</sub> |      |       | E <sub>ox</sub> |       | eV      | E <sub>CT</sub> ,<br>eV | $\Delta G_{\rm sol}$ eV | -ΔG <sub>cs'</sub><br>eV | –ΔG <sub>CR</sub> ,<br>eV |      |      |
|          |                       |                         |     |     |                       |                     |                  | -    | DPP   | TCBD            | TCBD  | Aniline | Aniline                 | -                       |                          |                           |      |      |
| 1        | 400                   | 477                     | 688 | 745 |                       | -                   | -                |      |       | -0.17           | -0.05 | 1.21    | 1.41                    | 1.60                    | 1.26                     | -0.40                     | 0.55 | 1.05 |
| 2        | 369                   | 472                     | 742 |     |                       | -                   |                  |      |       | -0.47           | -0.25 | 0.98    | 1.19                    | 1.57                    | 1.23                     | -0.40                     | 0.51 | 1.06 |
| 3        | 472                   | 630                     | 687 |     |                       | -                   |                  |      |       | -0.47           | -0.25 | 1.23    | 1.44                    | 1.68                    | 1.48                     | -0.26                     | 0.46 | 1.22 |
| 4        | 480                   | 535                     |     |     |                       | -                   |                  |      |       | -0.52           | -0.14 | 1.33    |                         | 2.17                    | 1.47                     |                           |      |      |
| 5        | 427                   | 560                     | 592 |     |                       | 65                  |                  | 1.35 | -1.04 |                 |       | 0.91    | 1.04                    | 1.99                    | 1.95                     |                           |      |      |
| 6        | 342                   | 455                     | 598 | 639 |                       | 688                 |                  | 1.31 | -0.97 |                 |       | 0.87    | 1.22                    | 1.87                    | 1.84                     |                           |      |      |
| 7        | 343                   | 396                     | 417 | 571 | 616                   | 638                 | 688              | 3.17 | -0.91 |                 |       |         |                         | 1.98                    |                          |                           |      |      |

Absorption and fluorescence spectral results in nonpolar toluene are depicted in Figure S22 with the summarized results in Table S1 in the supporting information. The spectral trends revealed subtle changes in their wavelengths, intensities, and lifetimes expected from the general solvation effect.

## **Electrochemistry and Spectroelectrochemistry**

Spectroelectrochemical studies combined with electrochemical redox studies were subsequently performed as they combinedly play a crucial role in characterizing electron transfer products, and more importantly, the occurrence of the intervalence phenomenon involving the target compound 1 in the present study. Depending on the level of interaction between the moieties in systems carrying two or more similar redox centers, the splitting of redox waves could be expected. This scenario applies to both the fully delocalized (class III type) and the in-between (class II) systems. However, as the redox centers are fully localized within the molecular framework for class I type systems, the redox potentials are expected to be identical, *ibid*, no splitting of the peak could be anticipated. In this case, the peak currents would be proportional to the number of redox-active entities at that potential. We have utilized both cyclic voltammetry

(CV) and differential pulse voltammetry (DPV) techniques in the present study; the former to address the reversibility of a given redox process and the latter to accurately obtain the peak potentials. Electrochemical studies were performed in o-dichlorobenzene (DCB) containing 0.1 M (TBA)ClO<sub>4</sub> (TBD = tetra-butyl ammonium) and the measured potentials are referenced to Ag/AgCl. DPV curves for studied systems are shown in Figure 3 while the oxidation and reduction potentials are tabulated in Table 1.

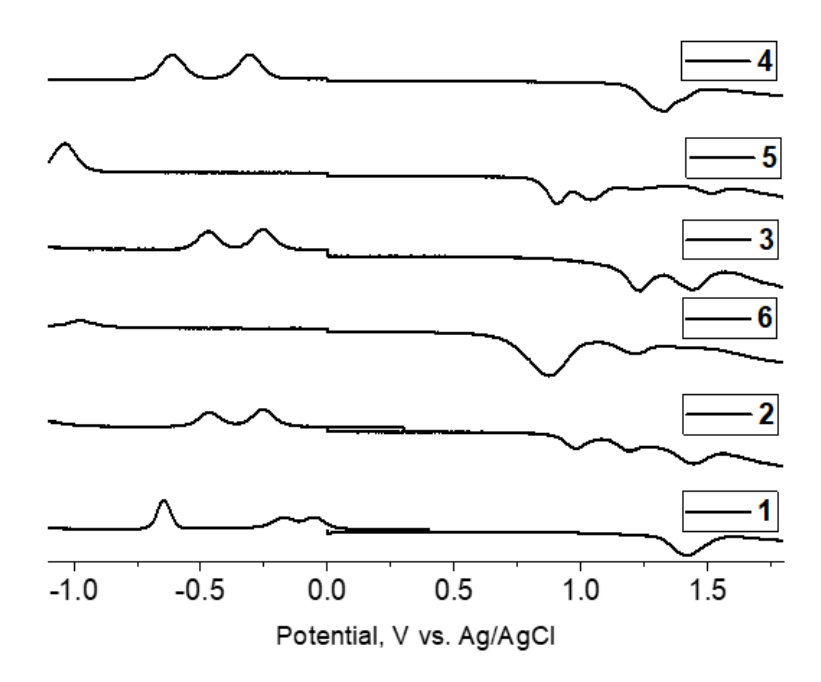


*Figure 3*. DPVs of 1-7 in o-dichlorobenzene containing 0.1 M (TBA)ClO<sub>4</sub>. Experimental conditions: scan rate = 5 mV/s, pulse width = 0.25 s, and pulse height = 25 mV.

Briefly, the control compound 7 having only TDPP revealed the first reduction at -0.86 V vs. Ag/AgCl. CV data confirmed this process to be quasi-reversible. The control compound 4 having DMA and TCBD entities revealed two reductions at -0.14 and -0.52 V due to the TCBD reductions and oxidation at 1.33 V for the DMA entity. Compounds 5 and 6, having DMA and TDPP entities but no TCBD, revealed the expected oxidation and reduction processes. By comparing the peak currents (one DMA in 5 against two DMAs in 6), the site of electron transfer to the DMA entity was possible to reach. For 5, a reduction at -1.04 V corresponding to TDPP, and oxidation at 0.91 V corresponding to DMA while for 6, a reduction at -0.97 for TDPP moiety, and oxidation at 0.87 V for DMA moiety were possible to assign. A slightly difficult reduction of TDPP compared to that observed for 7 due to the presence of electron-rich DMA was noted.

Molecular systems 2 and 3 comprised of three redox-active moieties displayed the expected redox processes. In the case of 3, TDPP reduction at -1.29 V, TCBD reductions at -0.25 and -0.47 V, and DMA oxidation at 1.23 V were detected. Similarly, for 2, a reduction at -1.22 V corresponding to TDPP, reductions at -0.25 and -0.47 V corresponding to TCBD, and DMA oxidations at 0.98 V (DMA entity distant from TCBD) and 1.19 V (DMA entity close to TCBD) was witnessed. In both compounds, the reduction of the TDPP entity was beyond -1.2 V, and also the TCBD reductions were easier by over 100 mV compared to 4 due to the inductive effects caused by the TDPP entity. Finally, target system 1 having two TCBD moieties coupled to TDPP revealed the expected split wave of the first reduction corresponding to TCBD. The split reductions appeared at -0.05 and -0.17 V (both reversible on the CV time scale) resulting in a 120 mV peak separation indicating the exchange of the odd electron among the TCBD moieties. Importantly, each peak approximately had about half the current predicted for simultaneous reduction of both TCBD moieties. The second reduction corresponding to the conversion of both  $TCBD^{-} \rightarrow TCBD^{2-}$ appeared at -0.67 V. In this case, the TDPP reduction in this compound was further cathodically shifted and appeared at -1.42 V while the DMA oxidation was anodically shifted to 1.21 V and was close to that observed for compound 4. In summary, although the electrochemical behavior of 1, (DMA-TCBD)<sub>2</sub>-TDPP, was similar to earlier reported (PTZ-TCBD)<sub>2</sub>-TDPP, the splitting was higher in the case of 1 indicating better electron exchange in the current system having DMA as terminal electron donors instead of PTZ.

Spectral features of the oxidized and reduced species of the investigated compounds were subsequently obtained using the spectroelectrochemical technique. Figure 4 displays the visible-near IR spectral changes during the course of the oxidation as well as the reduction processes of 1 and 2. The corresponding spectral changes for 3 are displayed in Figure S23 in SI. During the first oxidation of 1 (Figure 4a), the peak intensity of the neutral compound was decreased without developing any new peaks. On the contrary, during the reduction of 1, the diminished peak strength of the original compound was accompanied by intense new peaks at 1128 and 1454 nm (Figure 4b). The position of this peak was consistent with the intervalence charge transfer band reported earlier for (PTZ-TCBD)<sub>2</sub>-TDPP).<sup>72</sup> As shown in Figure 4 and Figure S23, for single TCBD-bearing compounds 2, and 3, as expected, no IVCT transition was observed. In these cases, both oxidized and reduced species had weak absorption in the region of 850 nm. For compounds, 5-6 lacking TCBD and 7 lacking both TCBD and DMA, no new spectral features were observed during

oxidation and reduction suggesting low molar absorptivity of any such transitions if at all they existed.

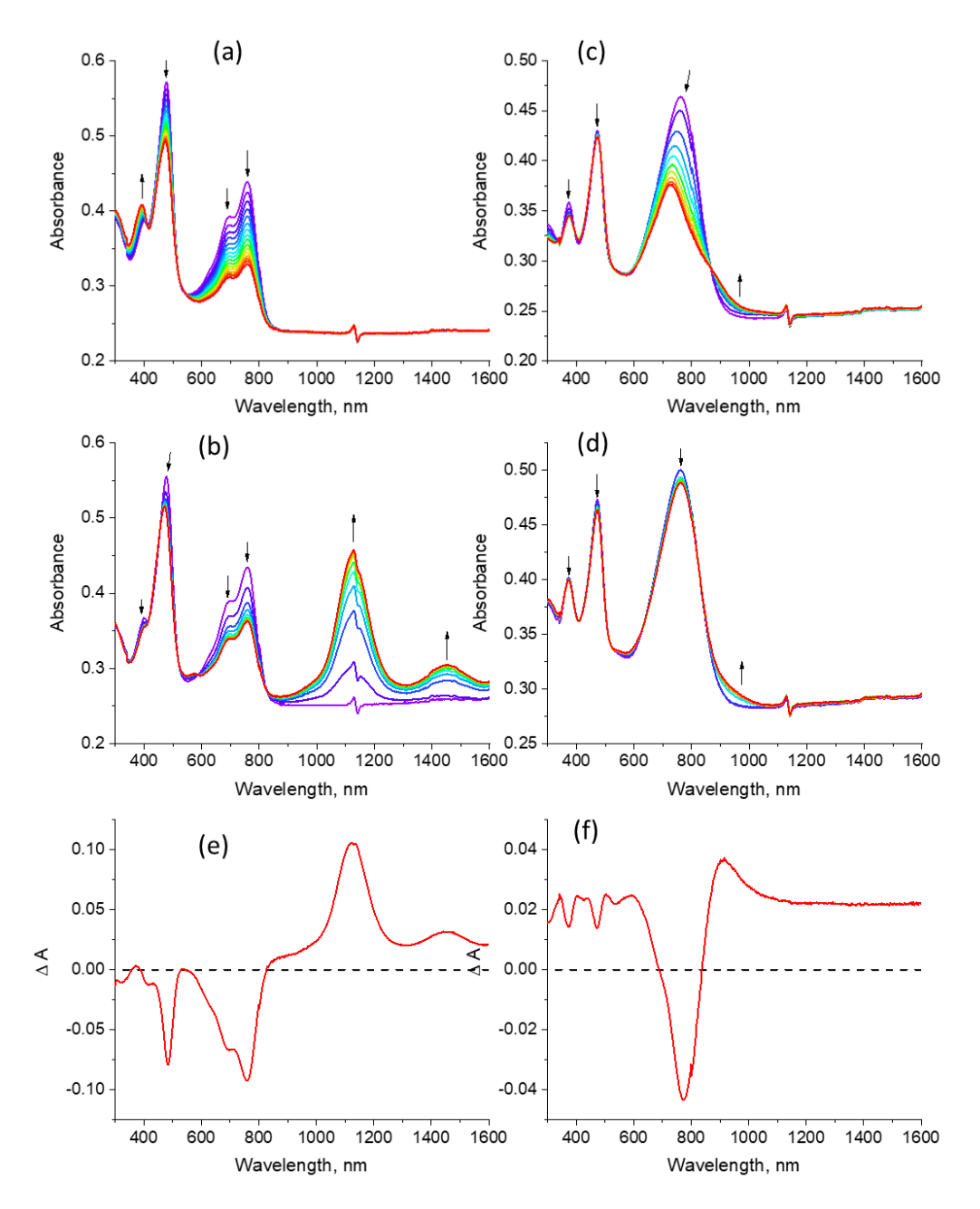


*Figure 4*. Visible-near-IR spectral changes during the course of the oxidation and reduction of 1 (a and b) and 2 (c and d) in DCB. The spectrum arrived for the charge-separated states (CSS) is depicted in Figures 4e and 4f, respectively, for 1 and 2.

The pair of reductions observed at -0.05 and -0.17 V in the case of  $\bf 1$  could be represented as,  $^{1-3,26}$ 

$$(DMA-TCBD)_2-TDPP \xrightarrow{e^-} DMA-TCBD^--TDPP-TCBD-DMA \xrightarrow{e^-} (DMA-TCBD^-)_2-TDPP$$

$$\downarrow IVCT$$

$$DMA-TCBD-TDPP-TCBD^--DMA$$
(i)

In here, the initial one-electron reduced anion radical mixed-valence species, capable of showing IVCT, is followed by its succeeding second electron reduction to the di-anionic species (both TCBDs in the reduced state). The potential difference of the split wave of  $\Delta E = 120$  mV imitates the energy associated with the dianion comproportionation, as shown by equation (ii).

$$1^{2-} + 1 \xrightarrow{K_{\text{Comp}}} 1^{-} + 1^{-} \tag{ii}$$

Further, the  $\Delta E$  value could also be used to evaluate the position of the equilibrium, as shown by equation (iii),

$$\Delta E = -\Delta G_{\rm com}/F \tag{iii}$$

where F is the Faraday constant and  $-\Delta G_{\text{com}}$  is the Gibbs free-energy change. Using this information, the stabilization of the radial anion can be estimated using equation (iv),

$$-\Delta G_{\text{com}} = -RT \ln K_{\text{com}}$$
 (iv)

Representing the electronic interactions between the 1/1- redox centers.<sup>26</sup> Using the potential difference between the split wave,  $\Delta E$  we calculated  $-\Delta G_{\rm com}$  according to equation (iii). Further, the calculated  $\Delta G_{\rm com}$  was used to calculate  $K_{\rm com}$  according to equation (iv). The calculated comproportionation equilibrium constant,  $K_{\rm com}$  and the stabilization energy,  $-\Delta G_{\rm com}$  from this procedure, were found to be 72.3 M<sup>-1</sup>, and 1.06 x 10<sup>4</sup> J/mol, respectively. The magnitude of these values was close to that reported earlier for (PTZ-TCBD)<sub>2</sub>-TDPP.

# Estimation of electronic coupling parameters from spectral and computational data

Energy-optimized structures of the investigated compounds were evaluated by DFT at the level of B3LYP/6-31G\* using *Gaussian 09*.<sup>74</sup> Additionally, to visualize the electronic structures, frontier HOMOs and LUMOs on the optimized structures using *GaussView* were subsequently generated. To save computational time, the N-C10 chain on the TDPP was replaced by ethyl.

Figure 5 shows the optimized structure along with frontier orbitals of 1 while others are shown in Figure S24 in SI, along with their energies listed in Table S2., No observable steric crowding was noted in these optimized structures. This becomes important when considering their close spatial dispositioning. For 1, the HOMO was localized on the central TDPP, and some contributions were on the TCBD while HOMO-1 was on the DMA entities. Expectedly, the LUMO and LUMO+1, distributed almost symmetrically on the TCBD-TDPP-TCBD portion were noted. Introducing solvents of differing polarity in these calculations, as shown in Figures S25-27 (see Table S2 for calculated energies of the orbitals), no notable changes in the distribution of the orbitals coefficients were observed, suggesting that the IVCT could appear in different solvents.

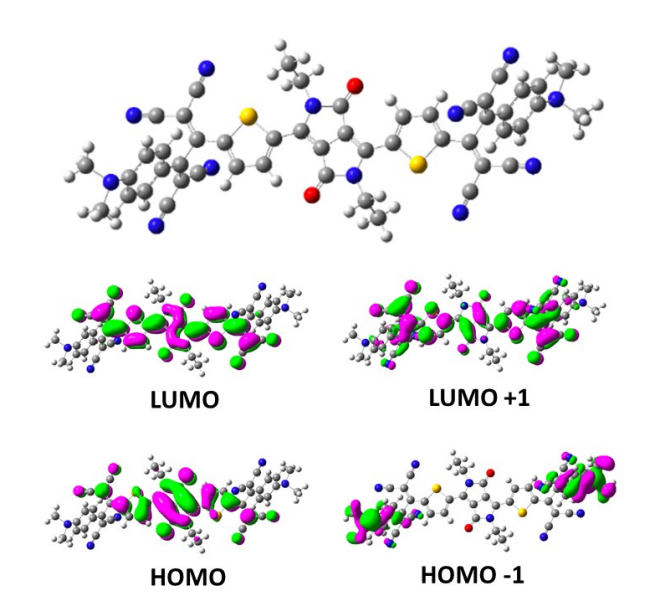


*Figure 5*. Geometry optimized structure and frontier HOMO-1, HOMO, LUMO, and LUMO+1 of 1, calculated at the B3LYP/6-31G\* level in the gas phase.

In contrast, for compounds 2, 3, 5, and 6, irrespective of the presence or absence of TCBD, the HOMO was found to be on TDPP while HOMO-1 was on the DMA entity. In the case of 5 and 6, LUMO was on TDPP while for 2 and 3, LUMO was on TDPP-TCBD parts of the molecules (Figure S24).

Further, the degree of electronic coupling was estimated by incorporating the computed structure into the e-Coupling Server program. (see Figures S28-29 and calculation details in SI). By this procedure, an estimated electron coupling ( $H_{AD} = 2V$ ) of 3.18 eV which was higher than the assessed  $\lambda$  of 1.60 eV (reorganization energy) was obtained. This suggests the current IVCT

molecule belongs to Class III. As pointed out earlier, compounds of Class III should be largely invariant of solvent polarity effects. To clarify this, cobaltocene, a chemical reducing agent was used to reduce 1 in different solvents. As exhibited in Figure S30, the peak position and shape of IVCT transition were essentially the same in dichlorobenzene, acetonitrile, and benzonitrile without major shifts in peak positions. These results support that 1 belongs to the class III type of IVCT compound. It is important to point out that the earlier reported system, (PTZ-TCBD)<sub>2</sub>-TDPP exhibited solvent-dependent IVCT peaks to some extent and thus was assigned to the in-between Class II and Class III types. It appears that changing the terminal electron donor from PTZ to DMA does have an effect on the intervalence phenomenon in this class of compounds.

Having established the occurrence of IVCT upon chemical or electrochemical reduction of 1, and further explaining the observed quenching of TDPP in 1, free-energy calculations to seek the thermodynamic possibility of excited-state charge separation was performed. Calculations of Gibbs free-energy on 1-3 possessing TCBD as accepted, TDPP as a sensitizer, and DMA as a donor was performed following to the traditional approach<sup>76</sup> (equations v-vi).

$$-\Delta G_{\rm CR} = E_{\rm ox} - E_{\rm red} + \Delta G_{\rm S} \tag{v}$$

$$-\Delta G_{\rm CS} = E_{\theta,\theta} - (-\Delta G_{\rm CR}) \tag{vi}$$

where  $E_{0.0}$  represents the excited energy of  $^{1}\text{TDPP*}$  and  $E_{\text{CT}}$  represents the charge transfer state energy, DMA $^{8+}$ -TCBD $^{8-}$  while  $\Delta G_{\text{S}}$  refers to solvation energy estimated by the dielectric continuum model (see equation iii). The oxidation potential of the donor and reduction potentials of the acceptor are represented by  $E_{\text{ox}}$  and  $E_{\text{red}}$ .

$$\Delta G_{\rm S} = -e^2/4 \pi \, \varepsilon_{\rm o} \, (R_{\rm cc} \, \varepsilon_{\rm R})^{-1}$$
 (iii)

The abbreviations  $\varepsilon_0$  and  $\varepsilon_R$  signify the vacuum permittivity and dielectric constant of PhCN used in photo- and electrochemical investigations ( $\varepsilon_R = 26.0$ ).  $R_{CC}$  is the center-to-center distance of the geometry-optimized structures between donor and acceptor entities. The calculated free-energy changes for both forward and reverse processes are listed in Table 1. These results evidently show the thermodynamic likelihood of excited-state charge separation and dark charge recombination.

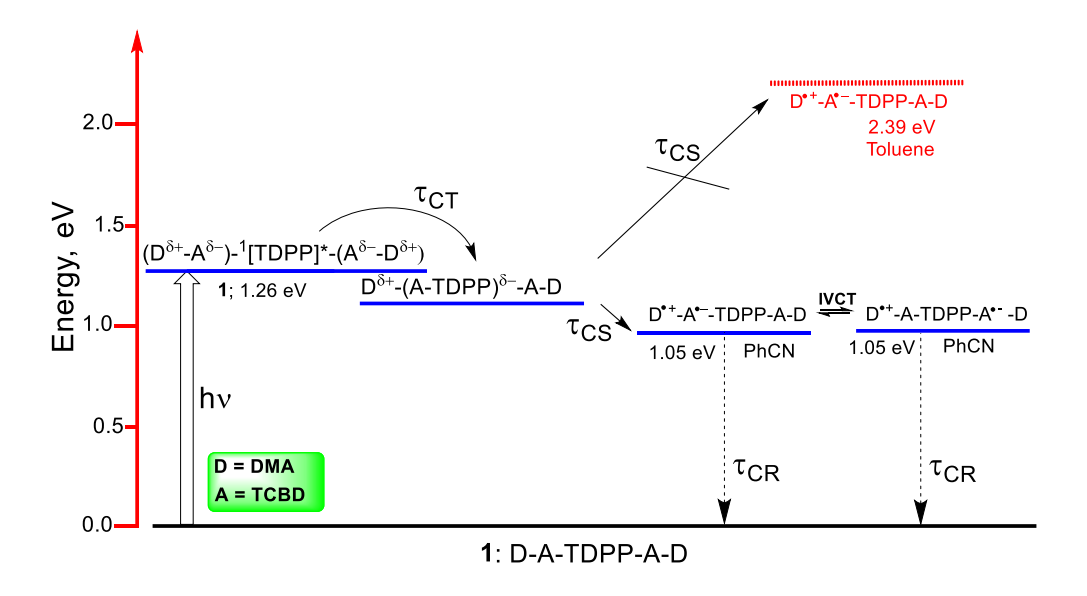


*Figure 6*. Jablonski-type energy level diagram showing excited-state CT and CS processes occurring in 1 in PhCN. The estimated energy of the CSS in toluene is also shown by dashed red lines.

By using the calculated free-energy change values, Jablonski-type energy level diagrams were built to envisage photoinduced events. Figure 6 shows the energy diagram for 1 while for 2 and 3 such energy diagrams are shown in Figure S31, and for 5 and 6 in Figure S32. For compounds 5 and 6 encompassed of electron-rich DMAs, and a relatively weak electron acceptor, TDPP,  $E_{0,0}$  (average of low-energy energy absorption and fluorescence peaks of <sup>1</sup>TDPP\*) were a little higher (~30-40 mV) than the electrochemical gap (difference between the first reduction and first oxidation potentials, see Table 1) signifying the possibility of CT occurrence (Figure S32). The previously presented fluorescence quenching and reduced lifetimes for these two compounds (see Table 1) draw support for this rationalization. The scenario changes when a much stronger electron acceptor, TCBD is introduced, as in compounds 1-3. The close spacing of TCBD to TDPP and high exergonicity would accelerate excited-state CT events. Further, in a polar PhCN, due to solvent stabilization of the radical ion pairs (charged cationic and anionic species), the initial charge transfer state is expected to undergo a full charge separation. Energetically, this seems to be the case as shown by the energy level diagrams in Figures 6 and S31. However, due to poor solvent stabilization in toluene, the formation of a charge-separated state appears unlikely (see reddashed lines in Figure 6). Under these situations, the charge transfer state could relax to the ground

state directly or populate the intermediate low-lying  $^3\text{TDPP*}$  ( $E_T = 1.04 \text{ eV}$ ) prior to relaxing to the ground state.

# Transient pump-probe absorption studies

In order to witness the envisioned charge transfer and separation events, femtosecond transient pump-probe spectral studies (fs-TA) covering the wide visible and near-IR regions were undertaken. Here, the samples were excited corresponding to their visible peak maxima. Figure S33 shows the fs-TA spectrum of only TDPP-bearing compound 7. Positive peaks at 779 and 891 nm and negative peaks at 570 and 630-640 nm were observed from the instantaneously formed <sup>1</sup>TDPP\* state within the first 1-2 ps. From the earlier discussed absorption and fluorescence spectra of TDPP (see Figure 7 for the inverse of these spectra for comparison), the 570 nm peak to ground state bleaching (GSB) and the negative peak in the 630-640 nm for both GSB and stimulated emission (SE) was assigned. Additionally, a wide peak covering the 805-1040 nm region (maxima at 890 nm) was observed and was ascribed to the absorption of excited state species (ESA) of the probe, <sup>1</sup>TDDP\*. The retrieval of GSB and SE transient peaks followed the decay of the ESA peaks persisted over 3 ns, the time delay window of the fs-TA instrument. This observation agrees with the earlier conversed long lifetime of 7 (3.17 ns).

Compounds **5** and **6**, having additional one or two entities of electron donor, DMAs to TDPP, exhibited spectral topographies sufficiently different from that of **7** (please see spectral results shown in Figure 7 in PhCN and Figure S34 in toluene). As predicted from the earlier discussed fluorescence lifetimes, recovery of the ESA peaks and the decay of GSB and SE peaks were sooner than that in **7**. Additionally, in the near-IR region, a new broad ESA peak (~1280 nm in benzonitrile and ~1464 nm in toluene) also appeared. As pristine TDPP exhibited no such ESA spectral features (Figure S33), and the energy calculations expected excited charge transfer, this near-IR peak was attributed to DMAδ--TDPPδ+.

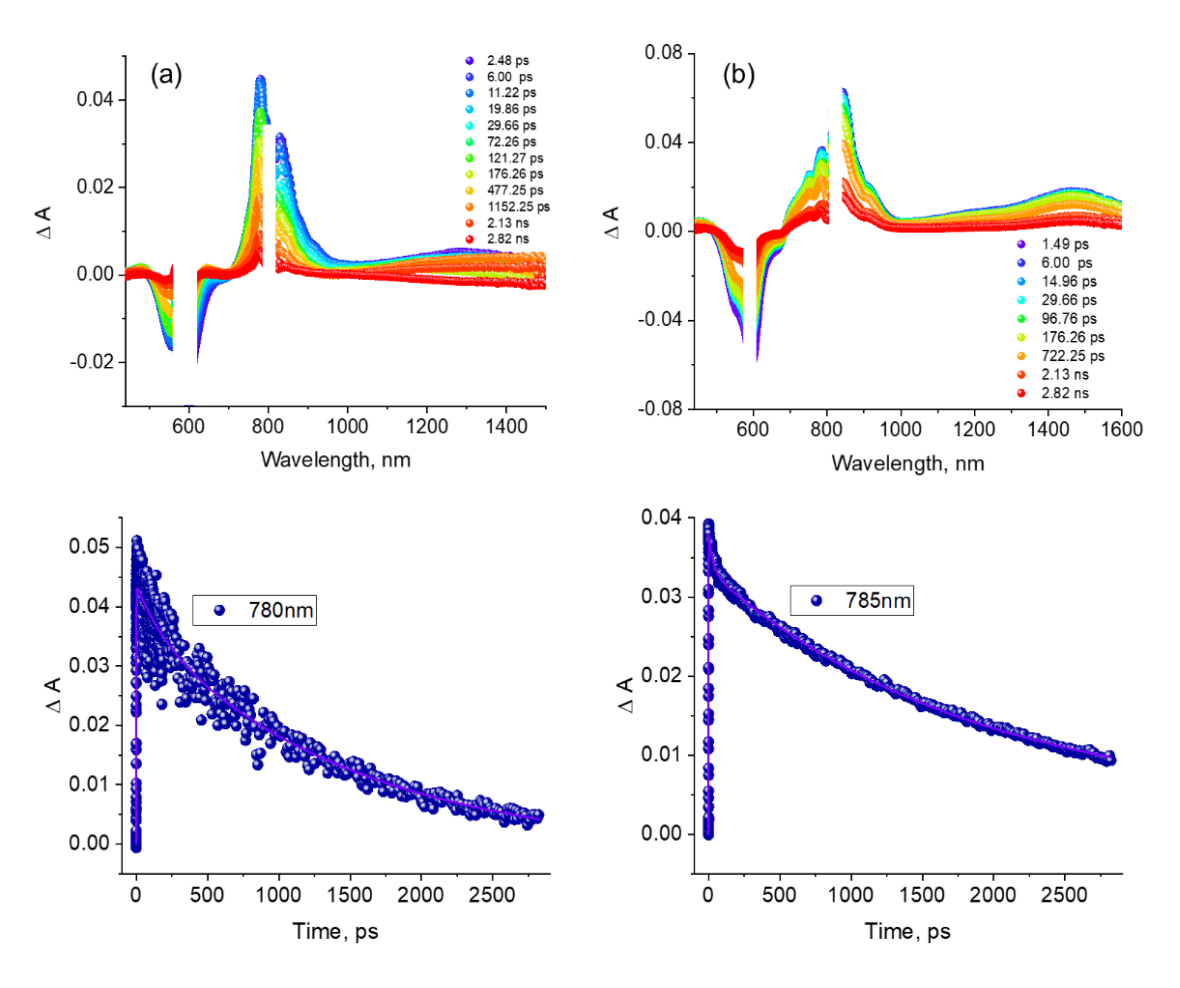


*Figure 7*. Transient spectra at the mentioned delay times of compounds (a) **5** and (b) **6** in PhCN (N<sub>2</sub>-purged). Excited was corresponding to their visible peak maxima (100 fs pulse width). The decay profile of the ESA peak is shown below each panel.

Lastly, after explaining all possible scenarios in these push-pull systems, we directed our attention to **1-3** having TCBD positioned between the DMA and TDPP. As demonstrated in Figures 2-6, for **1**, one could imagine the presence of an IVCT peak in the NIR region due to charge resonance between the electronically coupled TCBD entities after the charge separation process. Advantageously, the IVCT peak would help characterize the electron transfer product.

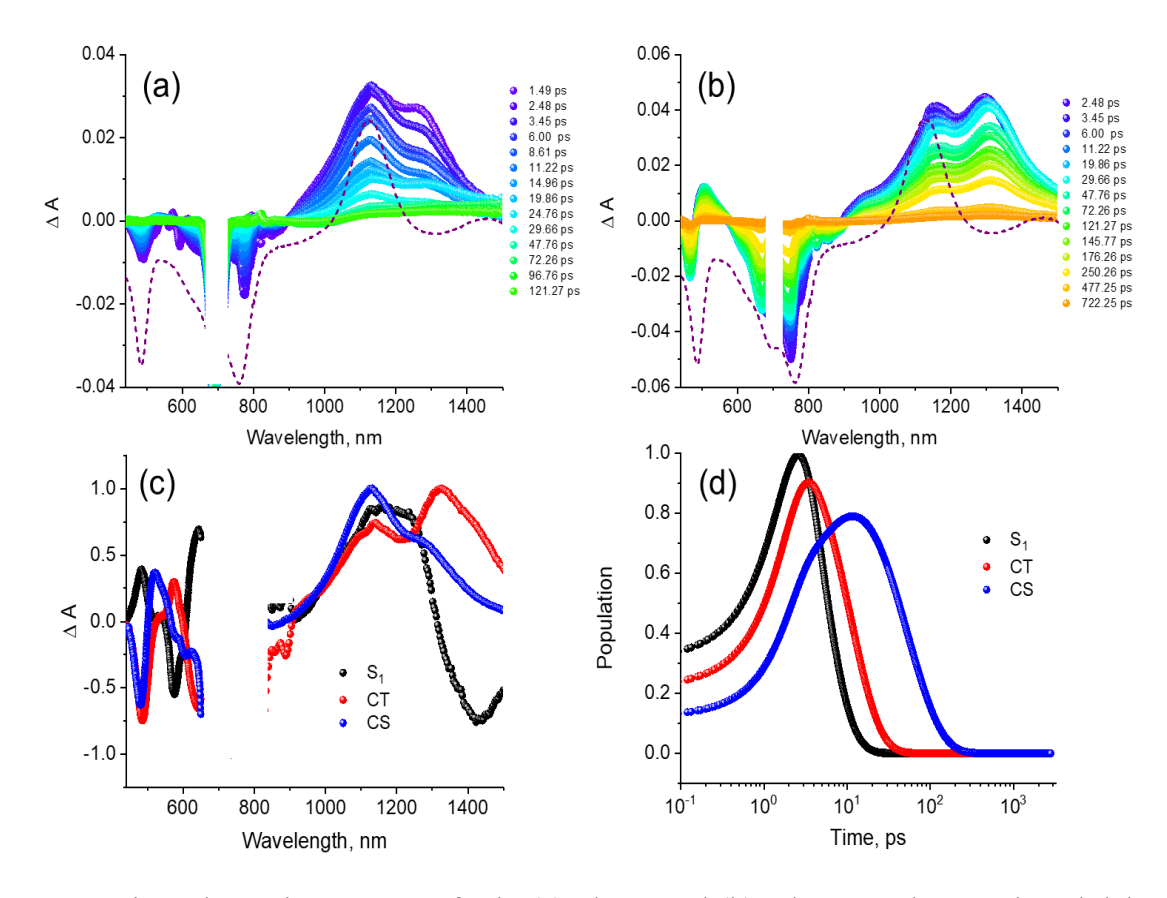


Figure 8. Transient absorption spectra of 1 in (a) PhCN and (b) toluene at the mentioned delay times. The dashed line indicates the spectrum of the CSS from spectroelectrochemistry. The species-associated spectra (SAS) and population kinetics are shown in c and d, respectively.

Figure 8a exhibits transient spectra of 1 in benzonitrile at the specified delay times. The spectrum deduced for the CSS from the spectroelectrochemical results is also incorporated for assessment determinations (dashed line). At 1.49 ps, the earlier delay time, the spectrum revealed negative peaks at 488, and 722 nm, and positive peaks at 1132 and 1266 nm. The decay of the 1266 nm peak was faster than the recovery of the negative peaks or that of the 1266 nm peak suggesting that this peak could be the intermediate CT state, DMA<sup>δ+</sup>-(A-TDPP)<sup>δ-</sup>-A-DMA, while the remaining peaks corresponding to the CS state, DMA·+-A·-TDPP-A-DMA undergoing charge resonance, DMA·+-A·-TDPP-A-DMA ←→ DMA·+-A-TDPP-A·-DMA. This becomes clear by comparing the spectrum of the CSS. These results back the occurrence of photo-excited charge separation resulting in IVCT via electron exchange between the two TCBD moieties. Further, the transient data was analyzed by feeding the data into the GloTarAn target analysis program.<sup>77</sup> For better data fitting, a sequential three-step process was warranted. The SAS for the three

d. The initial spectrum appearing around 5 ps could be attributed to <sup>1</sup>TDPP\* with contributions from vibrational cooling. The second one with a time constant of 7.87 ps revealed negative peaks at 485, 638, and 770 nm and positive peaks at 1140 and 1323 nm, and had features of the intermediate CT state, DMA<sup>δ+</sup>-(A-TDPP)<sup>δ-</sup>-A-DMA. The latter spectrum with a time constant of 49.2 ps exhibited the expected peaks for the CS intervalence state. Here, negative peaks at 478, and 772 nm and a positive peak at 1127 nm which matched well with the spectrum deduced from spectroelectrochemical results were witnessed.

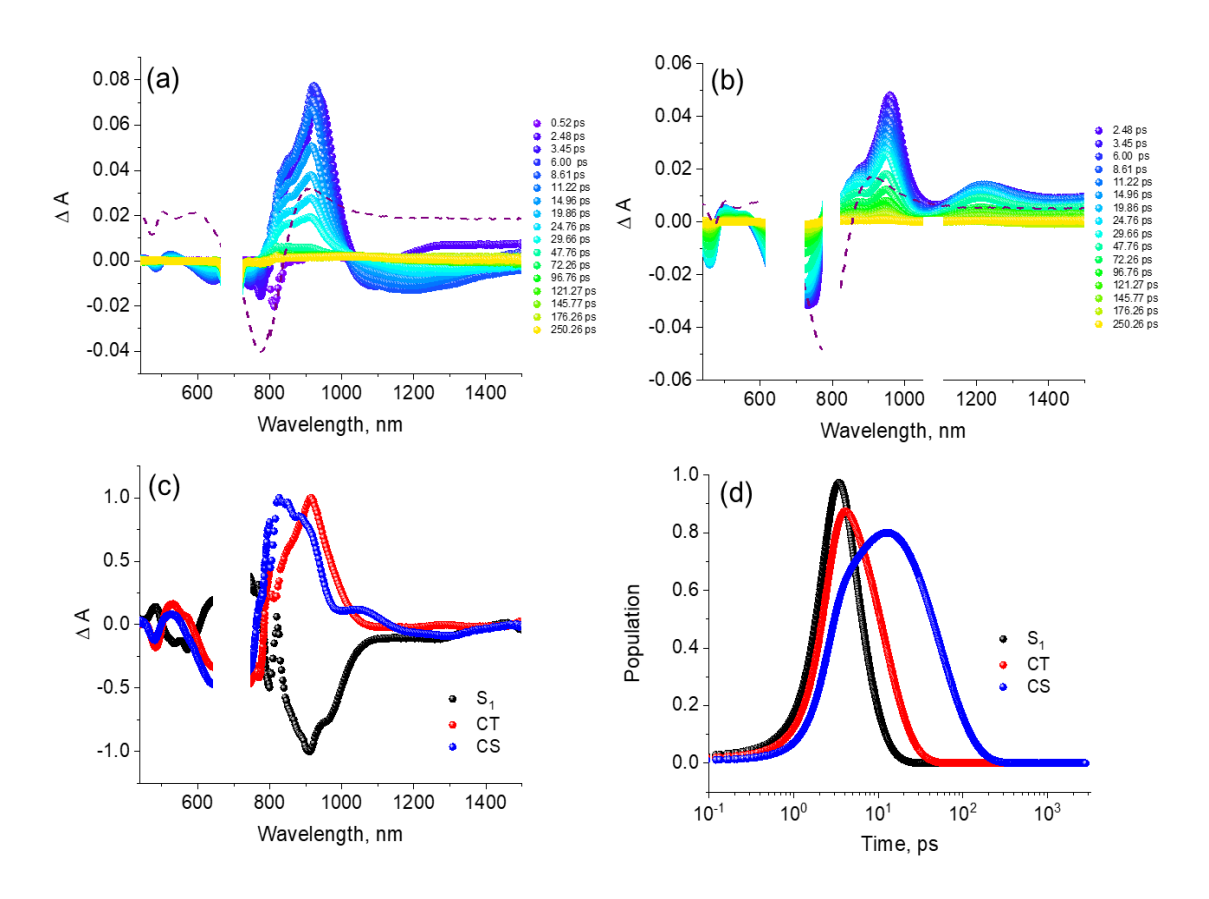


Figure 9. Fs-TA spectra of 2 in (a) benzonitrile and (b) toluene solvents at the indicated delay times. The dashed line shows the spectrum that arrived at the charge-separated state from spectroelectrochemistry. The SAS and their respective population time plots are respectively shown in c and d.

In contrast, the transient spectra in toluene revealed clearly different topographies from those detected in PhCN. The initial transient spectra were featured with negative peaks at 466, 470, and 752 nm and positive peaks at 1155 and 1301 nm (Figure 8b). Generally, the negative

peaks were blue-shifted and positive peaks were red-shifted (30-40 nm) when compared to the spectra in benzonitrile. Importantly, with time, the 1155 nm peak revealed a small decrease in intensity while increasing the intensity of the 1301 nm peak. Unlike that observed in PhCN, the peak attributed to the charge transfer state persisted longer time without any features in the 1132 nm range expected for the charge-separated species implying an absence of charge separation in toluene, an observation that readily agreed with the energy diagram in Figure 6.

**Table 2**. Kinetic time constants for CT and CR from GloTaAn analysis for **1-3** in the investigated solvents.

| System | λ <sub>ex</sub> , nm | Solvent | $\tau_{S1}$ , ps | τ <sub>CT</sub> , ps | τ <sub>CS</sub> , ps |
|--------|----------------------|---------|------------------|----------------------|----------------------|
| 1      | 700                  | PhCN    | 5.4              | 7.87                 | 49.21                |
|        |                      | Toluene | 0.31             | 8.41                 |                      |
| 2      | 700                  | PhCN    | 5.39             | 7.92                 | 49.33                |
|        |                      | Toluene | 0.26             | 7.01                 |                      |
| 3      | 687                  | PhCN    | 0.07             | 1.54                 | 65.39                |
|        |                      | Toluene | 0.95             | 15.15                |                      |

For single TCBD containing compounds **2** and **3**, the estimated Gibbs free-energy changes indicated the likelihood of CS. To clarify this, they were examined and the results are summarized in Figure 9 for **2** and Figure S35 for **3**. Immediately after excitation, compound **2** in benzonitrile revealed negative absorptions at 485, 643, and 775 nm and positive absorption at 921 nm along with a shoulder-type peak at 852 nm. Expectedly, the NIR IVCT peak was absent. With time the 921 nm peak underwent a blue shift of 8 nm, ultimately matching that expected for the CSS. However, in toluene, the positive peak located at 962 nm revealed only diminished intensity without showing any spectral shifts. These results collectively support the formation of CSS, DMA<sup>-+</sup>-A<sup>--</sup>-TDPP-DMA, from the intermediate DMA<sup>8+</sup>-(A-TDPP)<sup>8-</sup>-DMA CT state in the case of **2** in the utilized polar solvent but only the CT state in the nonpolar solvent. Similar spectral trends were also witnessed for **3** as shown in Figure S35, ibid, the formation of CSS, DMA<sup>-+</sup>-A<sup>--</sup>-TDPP from the intermediate DMA<sup>8+</sup>-(A-TDPP)<sup>8-</sup> in PhCN but only a CT state in toluene.

The transient data were subsequently analyzed using Glotaran target analysis, <sup>77</sup> and SAS and relevant kinetic data for both **2** and **3** were generated as shown in Figures 9c and d and S35, respectively. A sequential three-component fit in benzonitrile and ta wo-component fit in toluene provided satisfactory results. Data obtained from these analyses are given in Table 2 which shows a relatively fast charge transfer and separation process which could be rationalized to their close proximity.

# **Summary**

In conclusion, the investigated multi-modular push-pull system, 1 composed of TDPP, DMA, and TCBD was capable of exhibiting intervalence charge transfer upon either chemical or electrochemical reduction as well as in the product of photochemical charge separation. As observed for (PTZ-TCBD)<sub>2</sub>-TDPP, splitting of TCBD reduction wave in 1 was the primary evidence of charge resonance that was authenticated by spectro-electrochemical studies that exhibited the expected IVCT band in the NIR region. However, the IVCT peak position was solvent insensitive suggesting it belonged to a Type III intervalence compound. electrochemical data, the comproportionation equilibrium constant,  $K_{com}$ , and the stabilization energy,  $-\Delta G_{\text{com}}$ , were found to be 72.3 M<sup>-1</sup> and 1.06 x 10<sup>4</sup> J/mol, respectively. The assessed electronic coupling,  $H_{AD}$  was 3.18 eV, greater than  $\lambda$  of 1.60 eV, further confirming it to be a Class III type. The constructed energy diagrams facilitated further understanding of the photo events in the series of ICT systems. In PhCN, CT was followed by CS but only CT in nonpolar toluene was predicted. Comprehensive photophysical studies involving fs-TA were performed to prove solvent polarity dependence on charge transfer and separation events. Advantageously, the NIR IVCT band served as a marker to characterize the CT/CS product in 1. The CSS in 1-3 persisted for about 50-60 ps, signifying ultrafast processes due to geometric proximity and electronic communication between them.

#### ASSOCIATED CONTENT

# **Supporting Information**

The Supporting Information is available free of charge at <a href="https://pubs.acs.org/doi/xxxx">https://pubs.acs.org/doi/xxxx</a>.

<sup>1</sup>H and <sup>13</sup>C NMR, and MALDI-mass of synthesized compounds. Additional CVs and redox data, spectral data on neutral, oxidized, and reduced compounds, energy diagram, and fs-TA spectral data.

#### **AUTHOR INFORMATION**

### **Corresponding Authors**

# Rajneesh Misra

Department of Chemistry, Indian Institute of Technology, Indore 453552, India; orcid.org/0000-0003-3225-2125; Email: rajneeshmisra@iiti.ac.in

#### Francis D'Souza

Department of Chemistry, University of North Texas, 1155 Union Circle, #305070, Denton, TX 76203-5017, USA, orcid.org/0000-0003-3815-8949, E-mail: Francis.DSouza@UNT.edu

#### **Authors**

# Charu Popli

Department of Chemistry, Indian Institute of Technology, Indore 453552, India

# Youngwoo Jang

Department of Chemistry, University of North Texas, 1155 Union Circle, #305070, Denton, TX 76203-5017, USA

#### **Conflict of Interest**

There are no conflicts to declare.

#### **Author Contributions**

C.P and Y.J contributed equally to this work.

# Acknowledgments

This research was supported by the US-National Science Foundation (2000988 to FD), Council of Scientific and Industrial Research (Project No. CSIR 01(2934)/18/EMR-II) and (File number. 09/1022(0076)/2019/EMR-I), New Delhi and SERB (Project No. CRG/2018/000032) New Delhi, Govt. of India.

# **References and Notes**

- (1) Hankache, J.; Wenger, O. S. Organic mixed valence. *Chem. Rev.* **2011**, *111*, 5138-5178.
- (2) Heckmann, A.; Lambert, C. Organic mixed-valence compounds: A playground for electrons and holes. *Angew. Chem. Int. Ed.* **2012**, *51*, 326-392.
- (3) Hedley, G. J.; Ward, A. J.; Alekseev, A.; Howells, C. T.; Martins, E. R.; Serrano, L. A.; Cooke, G.; Ruseckas, A.; Samuel, I. D. W. Determining the optimum morphology in high-performance polymer-fullerene organic photovoltaic cells. *Nat. Commun.* **2013**, *4*, 2867-2876.
- (4) Lewis, I. C.; Singer, L. S. Electron spin resonance of radical cations produced by the oxidation of aromatic hydrocarbons with SbCl<sub>5</sub>. *Chem. Phys.* **1965**, *43*, 2712-2727.
- (5) Howarth, O. W.; Fraenkel, G. K. Electron spin resonance study of mono- and dimeric cations of aromatic hydrocarbons. *J. Am. Chem. Soc.* **1966**, *88*, 4514-4515.
- (6) Howarth, O. W.; Fraenkel, G. K. Electron spin resonance spectra of monomeric and dimeric cation radicals. *J. Chem. Phys.* **1970**, *52*, 6258-6267.
- (7) Launay, J. -P. Long-distance intervalence electron transfer. *Chem. Soc. Rev.* **2001**, *30*, 386-397.
- (8) Hush, N. S. *In mixed-valence compounds*; Brown, D. B., Ed.; D. Nato Science Series C, **1980**, *58*, 151-188.
- (9) Richardson, D. E.; Taube, H. Mixed-valence molecules: electronic delocalization and stabilization. *Coord. Chem. Rev.* **1984**, *60*, 107-129.
- (10) Nelsen, S. F.; Ismagilov, R. F.; Trieber, D. A. Adiabatic electron transfer: comparison of modified theory with experiment. *Science* **1997**, *278*, 846-849.
- (11) Creutz, C.; Taube, H. Direct approach to measuring the Franck-Condon barrier to electron transfer between metal ions. *J. Am. Chem. Soc.* **1969**, *91*, 3988-3989.
- (12) Creutz, C.; Taube, H. Binuclear complexes of ruthenium ammines. *J. Am. Chem. Soc.* **1973**, *95*, 1086-1094.
- (13) Demadis, K. D.; Hartshorn, C. M.; Meyer, T. J. The localized-to-delocalized transition in mixed-valence chemistry. *Chem. Rev.* **2001**, *101*, 2655-2686.
- (14) Creutz, C. Mixed valence complexes of d<sup>5</sup>-d<sup>6</sup> metal centers. *Inorg. Chem.* **1983**, *30*, 1-73.

- (15) Kaim, W.; Klein, A.; Glockle, M. Exploration of mixed-valence chemistry: Inventing new analogues of the Creutz-Taube Ion. *Acc. Chem. Res.* **2000**, *33*, 755-763; f) B. S. Brunschwig, C. Creutz, N. Sutin, *Chem. Soc. Rev.* **2002**, *31*, 168-184.
- (16) Brunschwig, B. S.; Sutin, N. Energy surfaces, reorganization energies, and coupling elements in electron transfer. *Coord. Chem. Rev.* **1999**, *187*, 233-254.
- (17) Alessandro, D. M. D'.; Keene, F. R. Current trends and future challenges in the experimental, theoretical and computational analysis of intervalence charge transfer (IVCT) transitions *Chem. Soc. Rev.* **2006**, *35*, 424-440.
- (18) Alessandro, D. M. D'.; Keene, F. R. Intervalence charge transfer (IVCT) in trinuclear and tetranuclear complexes of Iron, Ruthenium, and Osmium. *Chem. Rev.* **2006**, *106*, 2270-2298.
- (19) Launay, J. -P. Long-distance intervalence electron transfer. *Chem. Soc. Rev.* **2001**, *30*, 386-397.
- (20) Ward, M. D. Metal-metal interactions in binuclear complexes exhibiting mixed valency; molecular wires and switches. *Chem. Soc. Rev.* **1995**, *24*, 121-134.
  - (21) Aviram, A.; Ratner, M. A. Molecular rectifiers. Chem. Phys. Lett., 1974, 29, 277-283.
- (22) Song, H., Reed, M. A.; Lee, T. Single molecule electronic devices. *Adv. Mater.*, **2011**, 23, 1583-1608.
- (23) Solomon, G. C.; Andrews, D. Q.; Van Duyne, R. P.; Ratner, M. A. When things are not as they seem: quantum interference turns molecular electron transfer "rules" upside down. *J. Am. Chem. Soc.*, **2008**, *130*, 7788-7789.
- (24) Robin, M. B.; Day, P. Mixed valence chemistry-A survey and classification. Adv. *Inorg. Chem. Radiochem.* **1967**, *10*, 247-422.
- (25) Nelsen, S. F. "Almost Delocalized" Intervalence Compounds. *Chem. Eur. J.* **2000**, *6*, 581-588.
- (26) Hush, N. S. Intervalence-Transfer Absorption. Part 2. Theoretical Considerations and Spectroscopic Data, *Prog. Inorg. Chem.* **1967**, *8*, 391-443.
- (27) Bryce, M. R. Tetrathiafulvalenes as  $\pi$ -electron donors for intramolecular charge-transfer materials. *Adv. Mater.* **1999**, *11*, 11-23.
- (28) Verhoeven, J. W. On the role of spin correlation in the formation, decay, and detection of long-lived, intramolecular charge-transfer states. *J. Photochem. Photobiol C: Photochem. Rev.* **2006**, 7, 40-60.

- (29) Sun, D. L.; Rosokha, S. V.; Lindeman, S. V.; Kochi, J. K. Intervalence (charge-resonance) transitions in organic mixed-valence systems. Through-space versus through-bond electron transfer between bridged aromatic (redox) centers. *J. Am. Chem. Soc.* **2003**, *125*, 15950-15963.
- (30) Michinobu, T.; May, J. C.; Lim, J. H.; Boudon, C.; Gisselbrecht, J.; Seiler, P.; Gross, M.; Biaggio, I.; Diederich, F. A new class of organic donor–acceptor molecules with large third-order optical nonlinearities. *Chem. Commun.* **2005**, 737-739.
- (31) Kivala, M.; Boudon, C.; Gisselbrecht, J. -P.; Seiler, P.; Gross, M.; Diederich, F. Charge-transfer chromophores by cycloaddition–retro-electrocyclization: multivalent systems and cascade reactions. *Angew. Chem.* **2007**, *119*, 6473–6477.
- (32) Kivala, M.; Boudon, C.; Gisselbrecht, J. -P.; Seiler, P.; Gross, M.; Diederich, F. Chargetransfer chromophores by cycloaddition–retro-electrocyclization: Multivalent systems and cascade reactions. *Angew. Chem. Int. Ed.* **2007**, *46*, 6357-6360.
- (33) Gopinath, A.; Manivannan, N.; Mandal, S.; Mathivanan, N.; Nasar, A. S. Substituent enhanced fluorescence properties of star α-cyanostilbenes and their application in bioimaging. *J. Mater. Chem. B* **2019**, *7*, 6010-6023.
- (34) Michinobu, T.; Boudon, I.; Gisselbrecht, J. -P; Seiler, P.; Frank, B.; Moonen, N. N. P.; Gross, M.; Diederich, F. Donor-substituted 1,1,4,4-tetracyanobutadienes (TCBDs): new chromophores with efficient intramolecular charge-transfer interactions by atom-economic synthesis. *Chem. Eur. J.* **2006**, *12*, 1889-1905.
- (35) Michinobu, T. Adapting semiconducting polymer doping techniques to create new types of click post functionalization. *Chem. Soc. Rev.* **2011**, *40*, 2306-2316.
- (36) Shoji, T.; Ito, S.; Toyota, K.; Iwamoto, T.; Yasunami, M.; Morita, N. Reactions between 1-Ethynylazulenes and 7,7,8,8-Tetracyanoquinodimethane (TCNQ): preparation, properties, and redox behavior of novel azulene-substituted redox-active chromophores. *Eur. J. Org. Chem.* **2009**, 4316-4324.
- (37) Gotfredsen, H.; Neumann, T.; Strom, F. E.; Munoz, A. V.; Jevric, M.; Hammerich, O.; Mikkelsen, K. V.; Freitag, M.; Boschloo, G.; Nielsen, M. B. Donor–acceptor-functionalized subphthalocyanines for dye-sensitized solar cells. *ChemPhotoChem.* **2018**, *2*, 976-985.

- (38) Bui, A. T.; Philippe, C.; Beau, M.; Richy, N.; Cordier, M.; Roisnel, T.; Lemiegre, L.; Mongin, O.; Paul, F.; Trolez, Y. Synthesis, characterization and unusual near-infrared luminescence of 1,1,4,4-tetracyanobutadiene derivatives. *Chem. Commun.* **2020**, *56*, 3571-3574.
- (39) Yamada, M.; Schweizer, W. B.; Schoenebeck, F.; Diederich, F. Unprecedented thermal rearrangement of push–pull-chromophore–[60] fullerene conjugates: formation of chiral 1,2,9,12-tetrakis-adducts. *Chem. Commun.* **2010**, *46*, 5334-5336.
- (40) Yamada, M.; Rivera-Fuentes, P.; Schweizer, W. B.; Diederich, F. Optical stability of axially chiral push-pull-substituted buta-1,3-dienes: effect of a single methyl group on the C<sub>60</sub> surface. *Angew. Chem. Int. Ed.* **2010**, *49*, 3532-3535.
- (41) Sekita, M.; Ballesteros, B.; Diederich, F.; Guldi, D. M.; Bottari, G.; Torres, T. Intense ground-state charge-transfer interactions in low-bandgap, panchromatic phthalocyanine-tetracyanobuta-1,3-diene conjugates. *Angew. Chem. Int. Ed.* **2016**, *55*, 5560-5564.
- (42) Winterfeld, K. A.; Lavarda, G.; Guilleme, J.; Sekita, M.; Guldi, D. M.; Torres, T.; Bottari, G. Subphthalocyanines axially substituted with a tetracyanobuta-1,3-diene-aniline moiety: synthesis, structure, and physicochemical properties. *J. Am. Chem. Soc.* **2017**, *139*, 5520-5529.
- (43) Gautam, P.; Misra, R.; Thomas, M. B.; D'Souza, F. Ultrafast charge-separation in triphenylamine-BODIPY-derived triads carrying centrally positioned, highly electron-deficient, dicyanoquinodimethane or tetracyanobutadiene electron-acceptors. *Chem. Eur. J.* **2017**, *23*, 9192-9200.
- (44) Sharma, R.; Thomas, M. B.; Misra, R.; D'Souza, F. Strong ground- and excited-state charge transfer in C<sub>3</sub>-Symmetric truxene-derived phenothiazine-tetracyanobutadine and expanded Conjugates. *Angew. Chem. Int. Ed.* **2019**, *58*, 4350-4355.
- (45) Rout, Y.; Jang, Y.; Gobeze, H. B.; Misra, R.; D'Souza, F. Conversion of large-bandgap triphenylamine—benzothiadiazole to low-bandgap, wide-band capturing donor—acceptor systems by tetracyanobutadiene and/or dicyanoquinodimethane insertion for ultrafast charge separation. *J. Phys. Chem. C* **2019**, *123*, 23382-23389.
- (46) Poddar, M.; Jang, Y.; Misra, R.; D'Souza, F. Excited-state electron transfer in 1,1,4,4-Tetracyanobuta-1,3-diene (TCBD)- and cyclohexa-2,5-diene-1,4-diylidene-expanded TCBD-substituted BODIPY-phenothiazine donor-acceptor conjugates. *Chem. Eur. J.* **2020**, *26*, 6869–6879.

- (47) Pinjari, D.; Alsaleh, A. Z.; Patil, Y.; Misra, R.; D'Souza, F. Interfacing high-energy charge-transfer states to a near-IR sensitizer for efficient electron transfer upon near-IR irradiation. *Angew. Chem. Int. Ed.* **2020**, *59*, 23697-23705.
- (48) Yadav, I. S.; Alsaleh, A. Z.; Misra, R.; D'Souza, F. Charge stabilization *via* electron exchange: excited charge separation in symmetric, central triphenylamine derived, dimethylaminophenyl–tetracyanobutadiene donor–acceptor conjugates. *Chem. Sci.*, **2020**, *12*, 1109-1120.
- (49) Jang, Y.; Rout, Y.; Misra, R.; D'Souza, F. Symmetric and asymmetric push–pull conjugates: significance of pull group strength on charge transfer and separation. *J. Phys. Chem. B.* **2021**, *125*, 4067-4075.
- (50) Shinde, J.; Thomas, M. B.; Poddar, M.; Misra, R.; D'Souza, F. Does location of BF<sub>2</sub>-chelated dipyrromethene (BODIPY) ring functionalization affect spectral and electron transfer properties? Studies on α-, β-, and meso-functionalized BODIPY-derived donor–acceptor dyads and triads. *J. Phys. Chem. C* **2021**, *125*, 23911-23921.
- (51) Yadav, I. S.; Jang, Y.; Rout, Y.; Thomas, M. B.; Misra, R.; D'Souza, F. Near-IR Intramolecular charge transfer in strongly interacting diphenothiazene-TCBD and diphenothiazene-DCNQ push-pull triads. *Chem. Eur. J.* **2022**, e202200348.
- (52) Shoji, T.; Higashi. J; Ito, S.; Toyota, K.; Asao, T.; Yasunami, M.; Fujimori. K.; Morita, N. Synthesis and redox behavior of 1-azulenyl sulfides and efficient synthesis of 1,1'-biazulenes. *Chem. Eur. J.* **2008**, *8*, 1242-1252.
- (53) Winterfeld, K. A.; Lavarda, G.; Guilleme, J.; Guldi, D. M.; Torres, T.; Bottari, G. Subphthalocyanine–tetracyanobuta-1,3-diene–aniline conjugates: stereoisomerism and photophysical properties. *Chem. Sci.*, **2019**, *10*, 10997-11005.
- (54) Chen, J.; Cao, Y. Development of novel conjugated donor polymers for high-efficiency bulk-heterojunction photovoltaic devices. *Acc. Chem. Res.* **2009**, *42*, 1709-1718.
- (55) Cheng, Y. J.; Yang, S. H.; Hsu, C. S. Synthesis of conjugated polymers for organic solar cell applications. *Chem. Rev.* **2009**, *109*, 5868-5923.
- (56) Lin, Y.; Ma, L.; Li, Y.; Liu, Y.; Zhu, D.; Zhan, X. A solution-processable small molecule based on benzodithiophene and diketopyrrolopyrrole for high-performance organic solar cells. *Adv. Energy Mater.* **2013**, *3*, 1166-1170.

- (57) Lin, Y.; Li, Y.; Zhan, X. A solution-processable electron acceptor based on dibenzosilole and diketopyrrolopyrrole for organic solar cells. *Adv. Energy Mater.* **2013**, *3*, 724–728.
- (58) Qiao, Y.; Guo, Y.; Yu, C.; Zhang, F.; Xu, W.; Liu, Y.; Zhu, D. Diketopyrrole-containing quinoidal small molecules for high-performance, air-stable, and solution-processable n-channel organic field-effect transistors. *J. Am. Chem. Soc.* **2012**, *134*, 4084-408.
- (59) Berckstemmer, H.; Weissenstein, A.; Bialas, D.; Werthner, F. Synthesis and characterization of optical and redox properties of bithiophene-functionalized diketopyrrolopyrrole chromophores. *J. Org. Chem.* **2011**, *76*, 2426-2432.
- (60) Dhar, J.; Karothu, D. P.; Patil, S. Herringbone to cofacial solid state packing *via* H-bonding in diketopyrrolopyrrole (DPP) based molecular crystals: influence on charge transport. *Chem. Commun.* **2015**, *51*, 97-100.
- (61) Grzybowski, M.; Gryko, D. T. Diketopyrrolopyrroles: synthesis, reactivity, and optical properties. *Adv. Opt. Mater.* **2015**, *3*, 280-320.
- (62) Langhals, H.; Potrawa, T.; Nçth, H.; Linti, G. The influence of packing effects on the solid-state fluorescence of diketopyrrolopyrroles. *Angew. Chem. Int. Ed. Engl.* **1989**, *28*, 478-480.
- (63) Bold, G.; Duthaler, R. O.; Riediker, M. Enantioselective synthesis of D-threo-β-hydroxy-α-amino Acids with titanium-carbohydrate complexes. *Angew. Chem.* **1989**, *101*, 497-499.
- (64) Naik, M. A.; Patil, S. Diketopyrrolopyrrole-based conjugated polymers and small molecules for organic ambipolar transistors and solar cells. *J. Polym. Sci. Part A.* **2013**, *51*, 4241-4260.
- (65) Hartnett, P. E.; Margulies, E. A.; Mauck, C. M.; Miller, S. A.; Wu, Y.; Wu, Y.-L.; Marks, T. J.; Wasielewski, M. R. Effects of crystal morphology on singlet exciton fission in diketopyrrolopyrrole thin films. *J. Phys. Chem. B* **2016**, *120*, 1357-1366.
- (66) Mauck, C. M.; Hartnett, P. E.; Margulies, E. A.; Ma, L.; Miller, C. E.; Schatz, G. C.; Marks, T. J.; Wasielewski, M. R. Singlet fission *via* an excimer-like intermediate in 3,6-bis(thiophen-2-yl)diketopyrrolopyrrole derivatives. *J. Am. Chem. Soc.* **2016**, *138*, 11749-11761.
- (67) Huo, L. J.; Hou, J. H.; Chen, H. Y.; Zhang, S. Q.; Jiang, Y.; Chen, T. L.; Yang, Y. Bandgap and molecular level control of the low-bandgap polymers based on 3,6-dithiophen-2-yl-2,5-dihydropyrrolo[3,4-c]pyrrole-1,4-dione toward highly efficient polymer solar cells. *Macromolecules* **2009**, *42*, 6564-6571.

- (68) Walker, B.; Tomayo, A. B.; Dang, X. D.; Zalar, P.; Seo, J. H.; Garcia, A.; Tantiwiwat, M.; Nguyen, T. Q. Nanoscale phase separation and high photovoltaic efficiency in solution-processed, small-molecule bulk heterojunction solar cells. *Adv. Funct. Mater.* **2009**, *19*, 3063-3069.
- (69) Lin, Y. Z.; Cheng, P.; Li, Y. F.; Zhan, X. W. A 3D star-shaped non-fullerene acceptor for solution-processed organic solar cells with a high open-circuit voltage of 1.18 V. *Chem. Commun.* **2012**, *48*, 4773-4775.
- (70) Sahu, D.; Tsai, C. H.; Wei, H. Y.; Ho, K. C.; Chang, F. C.; Chu, C. W. Synthesis and applications of novel low bandgap star-burst molecules containing a triphenylamine core and dialkylated diketopyrrolopyrrole arms for organic photovoltaics. *J. Mater. Chem.* **2012**, *22*, 7945-7953.
- (71) Popli, C.; Jang, Y.; Patil, Y.; Misra, R.; D'Souza, F. Formation of highly efficient, long-lived charge separated states in star-shaped ferrocene-diketopyrrolopyrrole-triphenylamine donor–acceptor–donor Conjugates. *Chem. Eur. J.* **2020**, *26*, 15109-15115.
- (72) Khan, F.; Jang, Y.; Patil, Y.; Misra, R.; D'Souza, F. Photoinduced charge separation prompted intervalence charge transfer in a bis(thienyl)diketopyrrolopyrrole bridged donor-TCBD push-pull system. *Angew. Chem. Int. Ed.* **2021**, *60*, 20518-20527.
- (73) Principles of Fluorescence Spectroscopy, 3rd ed. (Ed.: J. R. Lakowicz), Springer, Singapore, **2006**.
- (74) Frisch, M. J.; Trucks, G. W.; Schlegel, H. B.; Scuseria, G. E.; Robb, M. A.; Cheeseman, J. R.; Scalmani, G.; Barone, V.; Mennucci, B.; Petersson, G. A., et. al. Gaussian 09, Revision A.1; Gaussian Inc.: Wallingford, CT, 2009.
- (75) De Vaca, I. C.; Acebes, A. S.; Victor, G. Ecoupling server: A tool to compute and analyze electronic couplings. *J. Comput. Chem.* **2016**, *37*, 1740-1745.
- (76) Rehm, D.; Weller, A. Kinetics of fluorescence quenching by electron and H-atom transfer. *Isr. J. Chem.* **1970**, *8*, 259-271.
- (77) Snellenburg, J. J.; Laptenok, S. P.; Seger, R.; Mullen, K. M.; van Stokkum, I. H. M. Glotaran: A java-based graphical user interface for the R Package TIMP *J. Stat. Softw.* **2012**, 49, 1-22. <a href="http://glotaran.org/">http://glotaran.org/</a> (date of access April 5, 2023)

# TOC graphic

